LEAKY-WAVE REGIMES ON MEMS-LOADED TRANSMISSION LINES FOR MM-WAVE APPLICATIONS

T. Zvolensky, D. Chicherin, A. V. Räisänen, and C. Simovski

Department of Radio Science and Engineering
SMARAD CoE, Aalto University (formerly TKK-Helsinki University of Technology)
P. O. Box 13000, AALTO FI-00076, Finland

Abstract—This paper presents study of controllable leaky wave modes in various planar transmission lines operating at millimetre wavelengths. Leaky wave regime is achieved by exploitation of periodic inclusions. The main goal is to obtain the scanning of the radiation angle from forward to backward direction and rather broad range of scanning angles at a given operation frequency corresponding to the mm-wave range. For this purpose, we suggest to use MEMS capacitors combined with shunt strap inductors. This design solution allows one to significantly reduce the losses in the loaded line compared to known scanning leaky-wave antennas based on varactors, or on magnetized ferrites. The design of the unit cell is done using global optimization method, and the dispersion is investigated analytically. After that, full wave analysis is done using Ansoft HFSS v.11 environment. After the leaky wave regimes are verified, an example of a leaky-wave antenna is introduced in order to confirm possibility of beam scanning.

1. INTRODUCTION

In recent years, several papers studying leaky-wave regimes in backward-wave structures have been published (see [1–3]). Among them there are papers (e.g., [1]) on leaky-wave modes in layered negative refractive index (NRI) materials. In [1], the authors use homogenization approach and present the solution in terms of the Green's function. However, NRI materials are in microwave frequency band practically periodic composites, and the accurate consideration should take into account their constituents. A periodically loaded

---

Corresponding author: T. Zvolensky (tomas.zvolensky@tkk.fi).
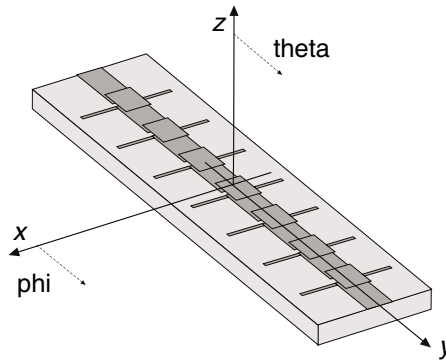
Figure 1. A sketch of a piece of suggested PLTL with its coordinate system.

planar transmission line (PLTL) is used in [2] to design a leaky wave coplanar waveguide (CPW) based slot antenna. The backward leaky wave regime allows this antenna to radiate with the negative angle (in Fig. 1 the radiation angle is scanned in zy plane, here negative angle means minus theta, with zero pointing in the direction of the z axis). Another example is excitation of leaky-wave on single and coupled microstrip interconnections [3]. Different approach to leaky-wave modes is the use of non-periodic (solid) substrates allowing to control the radiation direction (see, e.g., [4]). Exploiting special qualities of magnetized ferrites, i.e., the controllability of their permeability tensor using an electromagnet, the radiated beam can be scanned. However, losses in the ferrite material in the vicinity of the resonance are rather high (in the range of lower units of dB depending on the specific device, for further details, see [5]). The same (in the mm-wave range) refers to leaky-wave scanning antennas periodically loaded by varactors [6–8].

In this paper, we exploit the advantages offered by microelectromechanical (MEMS) capacitors which are controllable equivalents of simple coplanar strips from work [2]. This voltage-controlled variation of the capacitance results in the control of the radiation direction. This control is more efficient than that in [3] since the backward-wave regime can be engineered. Compared to [6–8], our design has significantly smaller losses (according to [9] MEMS loss is 0.05–0.2 dB in the wide frequency range, compared to varactors, which introduce insertion loss in the range of 0.3–1.2 dB due to soldering and ohmic losses). MEMS comprise metal portions and air gaps, there are no nonlinear and high-permittivity dielectric parts. Therefore, their array is more advantageous than ferrites and ferroelectric varactors, especially at millimetre wavelengths.

To engineer the needed phase velocities, which allow us to transit from forward to backward wave leakage, we need to combine capacitive and inductive loads. For our design parameters the homogenization model used in [2] is not valid. To come to the best possible design we first employ the analytical model of a transmission line periodically loaded by T-shaped circuits which has been suggested in [10]. After the initial design, we apply the global optimization algorithm-particle swarm optimization (PSO) [11]. Based on this analysis, CPW and MS unit cells are designed to fit imposed requirements. Full wave simulations taking into account the real geometry of MEMS and final optimization of these design solutions is done, and the controllable leaky wave regimes in these PLTL are confirmed.

2. ANALYTICAL MODEL

A unit cell of an infinite PLTL can be modeled as shown in Fig. 2(a). In this model, C_R and L_R represent characteristic values of capacitance and inductance of the host right-handed (RH) line per unit cell length, and C_L and L_L represent inserted periodical loads which are responsible for the dispersive behavior of PLTL at corresponding frequencies. The combination of these elements determines strongly dispersive character of PLTL, comprising the infinite number of such cells (see, e.g., [12]).

Another equivalent scheme of PLTL is shown in Fig. 2(b). It is significantly different from the one in Fig. 2(a), because it is implied that lumped Y and Z parameters refer only to lumped loads, parameters of unloaded transmission line are not displayed and are considered to be inherent. Since the host line portion between loads is not replaced by C_R and L_R parameters, this is not a homogenization model as that in Fig. 2(a) but a dynamic model [10] and can be used at higher frequencies than the model developed in [2]. In Fig. 2(b),
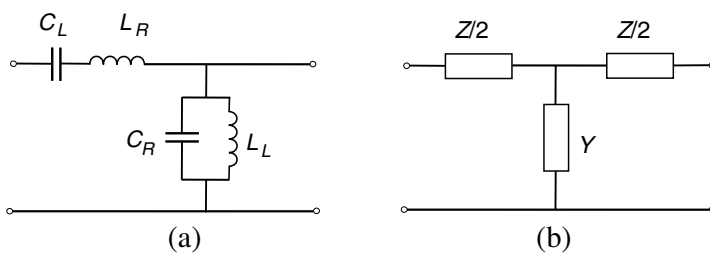
Figure 2. Models of PLTL unit cells. (a) Usual circuit model. (b) Tcircuit model.

loading impedances are in general form. For our case, the series impedance is replaced by capacitors and shunt admittance by inductor:

$$Z = \frac{1}{\eta \cdot j\omega C_L} \tag{1}$$

$$Y = \frac{\eta}{j\omega L_L}. \tag{2}$$

Here, η is the characteristic impedance of RH line. In the lossless case, this parameter can be expressed as:

$$\eta = \sqrt{\frac{L_R}{C_R}}. \tag{3}$$

Here, L_R and C_R are constitutive parameters of RH TL. Dispersion equation of any PLTL describing the dependency of propagation constant q on frequency can be written as [13]:

$$\cos(qa) = A. \tag{4}$$

Here, A is the first element of the transmission matrix of the PLTL unit cell [13]. For the case displayed in Fig. 2(b), the dispersion relation can be written as [10]:

$$\cos(qa) = \cos(ka) \cdot \left(1 + \frac{ZY}{4}\right) + \frac{j}{2} \cdot \sin(ka) \cdot \left(Z + Y + \frac{ZY^2}{4}\right) \tag{5}$$

where after introducing (1) and (2), we get:

$$\begin{aligned} \cos(qa) &= \cos(ka) \cdot \frac{4\omega^2 L_L C_L - 1}{4\omega^2 L_L C_L} \\ &+ \frac{1}{2}\sin(ka) \cdot \frac{4\omega^2 C_L \left(L_L + \eta^2 C_L\right) - 1}{4\eta\omega^3 L_L C_L^2}. \end{aligned} \tag{6}$$

In these formulas, a is the period of PLTL and k is the wavenumber in RH line, for which we can write:

$$k = \frac{\omega\sqrt{\epsilon_{eff}}}{c}. \tag{7}$$

Here, ϵ_{eff} is its effective permittivity of the substrate and c is the speed of light in vaccum. From (6) it is clear, that the loaded TL is strongly dispersive. It can support backward waves as well as forward ones.

Prior to numerical investigation of the dispersion, the loading parameters should be designed. For this purpose, PSO loop was implemented in Matlab to find parameters of RH TL (CPW and MS) and values of loading elements (i.e., MEMS capacitor and shunt inductor). Input vector of PSO loop contains many variables (width of the strip, gap between MEMS membrane and electrode, substrate

height and permittivity, etc.) and the error function is given by the resonant frequency and impedance of PLTL values differences. For detailed description of PSO, see [11].

The optimization procedure results into the dimensions of RH TL, MEMS capacitor and and shunt inductor (according to values of C_L and L_L). The study is done under two restrictions: that the loading elements should be electrically short in the direction along the line and that their values (i.e., capacitance of MEMS, shunt inductor inductance) should be practically realizable. The dispersion was investigated by solving (6) in Matlab. Dispersion diagrams for PLTLs with fixed loads can be seen in Fig. 3(a) (MS based) and in Fig. 3(b) (CPW based). In Fig. 3, we show the dispersion diagrams corresponding to initial-thick solid line (applied voltage corresponds to intermediate value of capacitance), maximal-thick dashed line (applied voltage is higher than for initial state) and minimal-thin dashed (applied voltage is smaller than for initial state) values of C_L for MEMS design shown in Figs. 5 and 6. Namely, $C_{\max} = 54\,\mathrm{fF}$, $C_{INIT} = 13\,\mathrm{fF}$, $C_{\min} = 9\,\mathrm{fF}$ (the capacitance calculation model can be seen in Fig. 4(a)).

Nevertheless, due to technological constraints, the ratio of marginal values of continually tunable MEMS capacitance can be maximally 1.5 in the case of a standard parallel plate MEMS varactor [9]. This is due to the fact that the upper membrane collapses to the lower electrode if the gap is lower than two thirds of its initial value. If a more sophisticated design is implemented, e.g., with an additional actuation electrode of small thickness compared to the thickness of the MS line (see Fig. 4(b)), the initial gap is thus larger
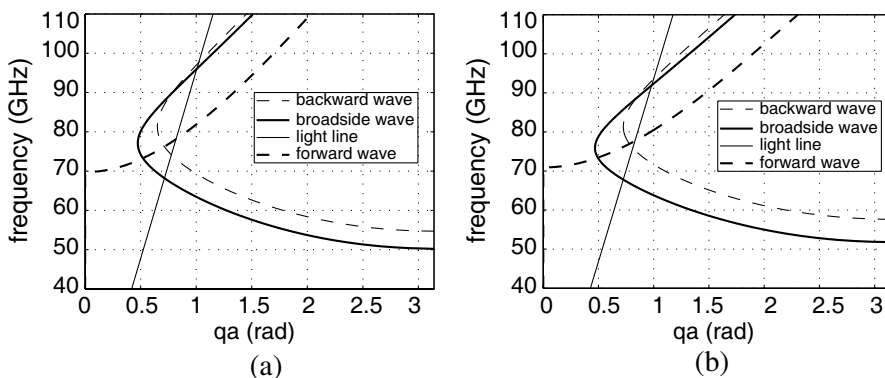
Figure 3. Analytical results. (a) Dispersion diagram of PL MS TL. (b) Dispersion diagram of PL CPW TL.
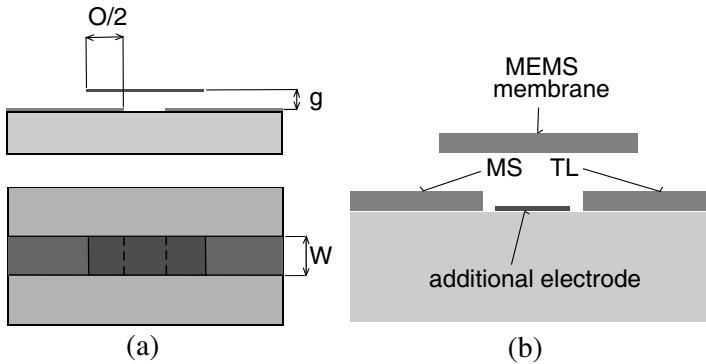
Figure 4. (a) MEMS capacitance calculation model: O is the overlapping area, g is the gap height and w is the width of TL. (b) Additional electrode sketch.
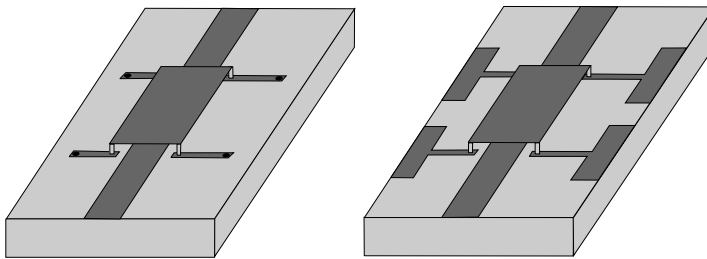
Figure 5. MS (left) and capacitively shorted MS (right) unit cell with MEMS stems model.

than the gap of the MEMS varactor. Consequently the capacitance ratio changes more than by a factor 1.5 if the gap between the membrane and actuation electrode changes to two thirds of its initial value. As a result the capacitance ratio can be increased to a value, e.g., 2, thus keeping the initial capacitance for broadside radiation, and $C_{\max} = 23.5$ fF and $C_{\min} = 11.5$ fF. The biasing network is not included in this early stage of the design (the models are done exactly as displayed in Figs. 5 and 6), so practicality of the design is connected to realizable values of MEMS capacitances. Thin solid line is the light line $\omega = q_0 c$ limiting the radiation (leaky-wave) region ($\beta < q_0$; note, that the wave number q is normalized by the period of unit cell, a). Geometrical parameters of unit cells are given in Section 4. Similarly, we calculated the parameters of MEMS for two other design solutions (based on CPW and based on CPS).

In Figs. 3(a) and 3(b), it can be seen that the main resonance for
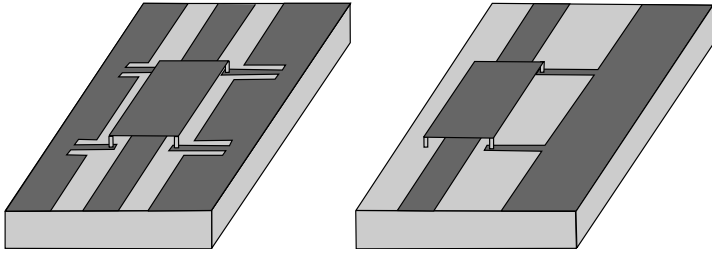
Figure 6. CPW (left) and CPS (right) unit cell with MEMS stems model.

capacitance C_{INIT} (zenithal wave) is centered at 77 GHz (the selected design frequency), at which the radiation direction would be zenithal. At higher frequencies the dispersion corresponds to the forward wave branch, and at lower frequencies to backward wave branch. Here we can clearly see that q is strongly dependent on C_L. When the capacitance varies between minimal and maximal values, the radiation direction at 77 GHz will change from backward to forward being zenithal for C_{INIT}. Dispersion diagrams for two other MEMS loaded TLs-coplanar strip line and grounded coplanar waveguide are similar to those displayed in Fig. 3 and thus not displayed.

Another important parameter of metamaterial unit cells is the Bloch impedance, which is the characteristic impedance at the gates of the unit cell. After solving the matrix equation connecting currents and voltages at the enterance and outpout of the unit cell (using transmission matrix), the Bloch impedance can be defined as [16]:

$$Z_B = \frac{-BZ_0}{A - e^{\gamma a}}. \tag{8}$$

Here, A and B are components of general two port transmission matrix components, Z_0 is the characteristic impedance of the host TL and $e^{\gamma a}$ is the propagation factor by which the voltages and currents differ at the gates of infinately long PLTL. After further simplification — for symmetrical unit cell, which is our case, we get [16]:

$$Z_B^{\pm} = \frac{\pm BZ_0}{\sqrt{A^2 - 1}}. \tag{9}$$

Expressing the Bloch impedance in terms of resonance frequencies of serial and parallel resonators formed by the paramters of the host

TL and loading elements (8) reduces to [13]:

$$Z_B = \sqrt{\frac{(\omega/\omega_{SE})^2 - 1}{(\omega/\omega_{PA})^2 - 1} - \left\{\frac{\omega_L}{2\omega}\left(\left[\frac{\omega}{\omega_{SE}}\right]^2 - 1\right)\right\}^2}. \quad (10)$$

Here, ω is the resonant frequency of the unit cell (77 GHz), ω_{SE}, ω_{PA} and ω_L are defined as (according to Fig. 2(a)):

$$\omega_{SE} = \frac{1}{\sqrt{C_L L_R}} \qquad \omega_{PA} = \frac{1}{\sqrt{C_R L_L}} \qquad \omega_L = \frac{1}{\sqrt{C_L L_L}}. \quad (11)$$

Calculating the Bloch impedance analytically, using (10), the result can be seen in Figs. 7 and 8 for MS and CPW based unit cells.
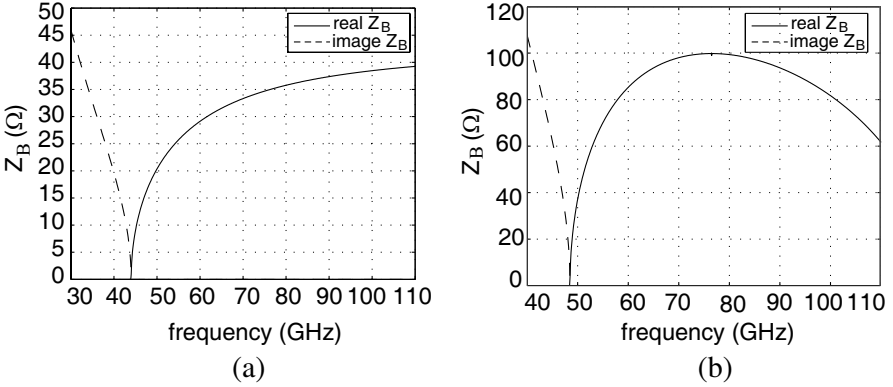
Figure 7. Analytical results. (a) The Bloch impedance of MS based unit cell. (b) The Bloch impedance of CPW bsed unit cell.
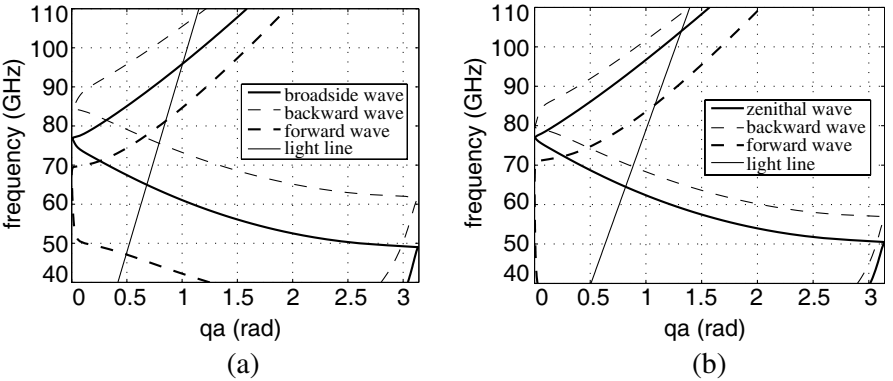
Figure 8. Full wave simulation results. (a) Dispersion of PL MS TL. (b) Dispersion of PL CPW TL.
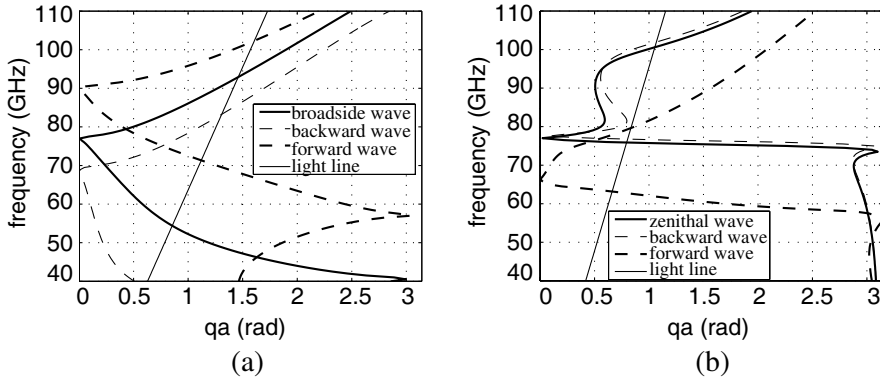
Figure 9. Full wave simulation results. (a) Dispersion of PL CPS TL. (b) Dispersion of PL capacitively shorted MS TL.

3. FULL WAVE SIMULATIONS OF CPW AND MS UNIT CELLS

The actual models of simulated unit cells are shown in Figs. 5 and 6. Here, the C_R and L_R are inherent to the particular TL type, and calculated based on conformal mapping approximation. Capacitance C_L is created by the MEMS model, i.e., membrane over the TL with gap in the middle. Since the full-wave model takes into account the real geometry of MEMS with four stems shown in Figs. 5 and 6, this study gives the verification of possibility to excite leaky-wave modes in MEMS-loaded TL and serves also for the validation of the analytical model. Full wave analysis is done using Ansoft HFSS v.11. The initial geometric parameters of the unit cell structure are obtained from previously mentioned PSO code. By fine variation of the model parameters we obtain results similar to the analytical ones and see that the initial analytical model gives the acceptable accuracy. Its error is mainly related to shift of the resonance frequency.

Final (for optimal PLTL) results of simulations can be seen in Figs. 8 and 9 for all considered types of TLs, though in Fig. 9(b), the dispersion curve for zenithal and backward wave behaves differently. This only shows, that the structure is more sensitive on the change of capacitance of MEMS (resonant frequency and forward and backward branches are still available). These results clearly show that for all types of considered TLs, the resonance frequency (for initial MEMS capacitance) can be placed at the required design frequency 77 GHz with the zenithal radiation for C_{INIT} and that the forward and backward wave leakage is realizable within realistic MEMS
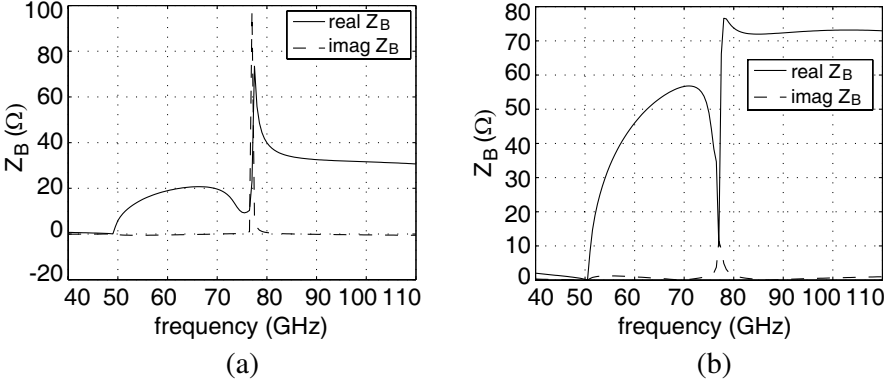
Figure 10. Full wave simulation results. (a) The Bloch impedance of MS based unit cell. (b) The Bloch impedance of CPS based unit cell.

capacitances limits. In later stages, MEMS will be fabricated based on technology used in [15], where the capacitance of MEMS is tunable quasi-continuously. For extraction of Bloch impedance, the relation between transmission and scattering paramters has been used, final formula used has been [13]:

$$Z_B = \frac{2jZ_0 S_{21} \sin(qa)}{(1 - S_{11})(1 - S_{22}) - S_{21}S_{12}}. \tag{12}$$

In Fig. 10(a), is displayed the Bloch impedance for MS based unit cell. We can see strong resonance around the design frequency, i.e., 77 GHz. This would suggest, that the unit cell does not work in balanced regime, nevertheless, the resonance is caused by numerical error, since the balanced regime is extremely narrow banded, so even the smallest deviation from the balanced state causes this resonant behavior of the Bloch impedance. After interpolation of the data around the resonance peak, it can be seen that the Bloch impeadance at 77 GHz is practically the same (for MS based unit cell), when compared to analytical calculation. As for the CPW based unit cell, the result of numerical simulation can be seen in Fig. 10(b), where after the interpolation, the difference between the analytical and numerical calculation is larger, nevertheless, the overall accuracy is sufficient.

4. LEAKY-WAVE REGIMES FOR FINITE PLTL

The purpose of this section is to verify the applicability of the design procedure used in previous sections. By stacking a finite number of
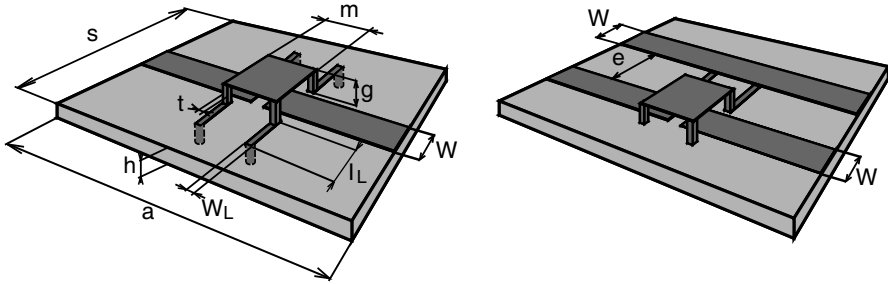
Figure 11. MS unit cell dimensions (left) and CPS cell dimensions (right; displayed only dimensions different from MS cell).

designed unit cells, we obtain a periodical structure, which comprises leaky-wave antenna (LWA). It is clear, that to realize the leaky wave regime with the main direction of radiation predicted in the previous section one needs the matched termination. However, there is no evidence that this solution is optimal for any number N of unit cells. First, the directivity is proportional to the PLTL length, i.e., to N. Second, in this matched design case a significant part of the applied power is lost in the matching resistance. Therefore, we impose the requirement of the high enough gain in the main lobe ($\geq 1\,\text{dB}$), 50% overall antenna efficiency and acceptable pattern (maximum of side-lobes below $-5\,\text{dB}$ compared to the main lobe). These conditions lead us to the design with the open-end termination. The geometrical parameters (corresponding to Fig. 11) of the final design are as follows:

1. MS-based design: length of unit cell $a = 600\,\mu\text{m}$, strip width $w = 30\,\mu\text{m}$, width of the split in the strip under the membrane $gap = 100\,\mu\text{m}$, width of the whole structure $s = 1100\,\mu\text{m}$, MEMS membrane height over the strip $g = 3\,\mu\text{m}$, membrane length $m = 202\,\mu\text{m}$, MEMS stem thickness $t = w_L = 5\,\mu\text{m}$, strap length $l_L = 340\,\mu\text{m}$ and width $w_L = 5\,\mu\text{m}$, substrate thickness $h = 179\,\mu\text{m}$ and permittivity of substrate 7 (silicon nitride).

2. CPS-based design: length of unit cell $a = 750\,\mu\text{m}$, strips width $w = 218\,\mu\text{m}$, gap between strips $e = 150\,\mu\text{m}$, width of the whole structure $s = 2586\,\mu\text{m}$, MEMS membrane height $g = 1.8\,\mu\text{m}$, membrane length $l = 110\,\mu\text{m}$, stem thickness $t = 17\,\mu\text{m}$, strap length $l_L = 150\,\mu\text{m}$ and width $w_L = 17\,\mu\text{m}$, substrate thickness $h = 145\,\mu\text{m}$ and permittivity of substrate 8. Losses in the dielectric substrate (loss tangent 0.006) are taken into account. The influence of metal losses has been checked and it turned out to be minor. Therefore in further simulations the PEC approximation has been used.
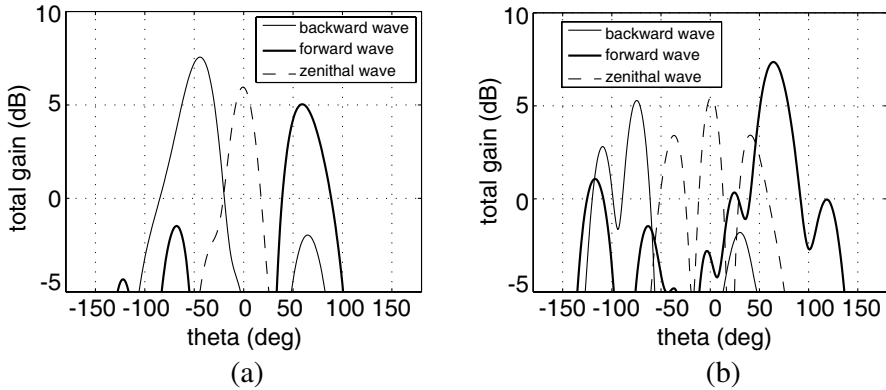
Figure 12. Radiation patterns of LWA. (a) MS line based LWA, open ended termination. (b) CPS based LWA.

Radiation patterns for yz plane (see Fig. 1) are depicted in Fig. 12. Thin dashed curve represents the pattern for initial value of MEMS capacitance. Thin solid and thick solid curves correspond to minimal and maximal capacitances, respectively. The design with the MS line is clearly better. The main beam is well pronounced and does not contain significant dips. The total angle of scanning is nearly $130°$ (from $-80°$ to $+50°$) and for all values of the MEMS capacitance the side-lobe maxima are nearly $10\,\text{dB}$ less than the main lobe maximum. For practically realizable MEMS maximal and minimal capacitances ratio equal to 2 (mentioned in Section 2), the range of angles reduces, i.e., from $-22°$ to $21°$, which is satisfactory with regard on required gain values. High sidelobes level (Fig. 12(b)) could be caused by possible excitation of bound and leaky modes at the same time resulting into difficulties while designing final structure. Nevertheless, the purpose of these patterns is to show the possibility to steer the angle of the main beam radiation.

The parameters of the structure can be further improved — the directivity by stacking more cells in row, and sidelobes level by increasing the width of the structure. Further improvement of the sidelobes level can be achieved by investigating the radiation of the stub inductors, whereas strong currents flowing through them can cause some radiation, which is significantly affecting the sidelobes level.

5. CONCLUSION

We have suggested a new design solution for transmission lines operating in leaky-wave regime as a scanning leaky-wave radiating system. This soulution is based on the use of MEMS combined with shunt strap inductors, i.e., we apply the periodical loading of the line by resonant circuits. A study of dispersive properties of three types of controllable periodically loaded transmission lines is done for realistic MEMS parameters, where the loads combine MEMS capacitors and strap inductors. The investigation shows that these PLTL structures support forward and backward leaky waves in the balanced regime (no stop-band at the point of zero phase velocity). This opens the possibility, e.g., to the scanning of leaky-wave's radiated beam around the zenithal direction. After preliminary design and optimization based on analytical modeling of PLTL, full wave simulations taking into account the realistic geometry of MEMS with four stems are done. After minor revision of analytically optimized parameters we obtain numerically optimized unit cells for all three types of the host line we study in this paper. From simulations, it is clear that leaky-wave regimes in the mm wavelength range are feasible for a certain range of MEMS capacitances. Therefore MEMS-loaded TL can be used for efficient electric steering of LWA. The advantage of MEMS such as low losses and sufficient coverage of available capacities allow one to make these antennas highly efficient. Simulations of structures comprised of stacked MS and CPS unit cells are done for the open-end design which ensures the good overall antenna efficiency. In spite of the obvious reflected wave in the loaded transmission line the maximum of the main lobe is still directed in accordance with the dispersion in the infinite PLTL: minimal capacitance of MEMS provides radiation to the backward direction, the initial capacitance to the zenithal direction and the maximal capacitance to the forward direction.

ACKNOWLEDGMENT

REFERENCES

1. Bagley, Q., B. Wu, and L. Tsang, "Electromagnetic fields of hertzian dipoles in layered negative refractive index materials," *IEEE Antennas Wirel. Propag. Lett.*, Vol. 7, 749–752, 2008.

2. Grbic, A. and G. V. Eleftheriades, "Leaky CPW-based slot antenna arrays for millimeter-wave applications," *IEEE Trans. Antennas Propag.*, Vol. 50, No. 11, 1494–1504, 2002.

3. Hanson, G. W. and A. B. Yakovlev, "Leaky wave excitation on three-dimensional printed interconnects," *IEEE MTT-S Digest*, Vol. 2, 499–502, 2004.

4. Diamantis, S. G., G. A. Kyriacou, A. A. Mavrides, and J. N. Sahalos, "Investigation of eigen-backward and leaky-waves modes of an axially magnetized lossy cylindrical ferrite substrate," *XXVIIth General Assembly of the International Union of Radio Science*, No. 1270, 17–24, Maastricht, Aug. 2002.

5. Subramanyam, G., F. Ahamed, R. Biggers, R. Neidhard, E. Nykiel, J. Ebel, R. Strawser, K. Stamper, and M. Calcatera, "RF performance evaluation of ferroelectric varactor shunt switches," *Microwave Opt. Technol. Lett.*, Vol. 47, No. 4, 370–374, 2005.

6. Gil, I., J. Bonache, J. García-García, F. Martín, and R. Marqués, "Tunable split ring resonators for reconfigurable metamaterial transmission lines," *IEEE Trans. Microwave Theory Tech.*, Vol. 54, No. 6, 2665–2674, 2006.

7. Öjefors, E., S. Cheng, K. From, I. Skarin, P. Hallbjörner, and A. Rydberg, "Electrically steerable single-layer microstrip traveling wave antenna with varactor diode based phase shifters," *IEEE Trans. Antennas Propag.*, Vol. 55, No. 9, 2451–2460, 2007.

8. Piazza, D., M. D'Amico, and K. R. Dandekar, "Two port configurable CRLH leaky wave antenna with improved impedance matching and beam tunning," *Proc. of the European Conference on Antennas and Propagation*, 2046–2049, Berlin, March 23–27, 2009.

9. Rebeiz, G. M., *RF MEMS Theory, Design, and Technology*, John Wiley & Sons, Inc. Publication, 2003.

10. Simovski, C., "Bloch material parameters of magneto-dielectric metamaterials and the concept of Bloch lattices," *Metamaterials*, Vol. 1, No. 2, 62–80, 2007.

11. Robinson, J. and Y. Rahmat-Samii, "Particle swarm optimization in electromagnetics," *IEEE Trans. Antennas Propag.*, Vol. 52, No. 2, 397–407, 2004.

12. Caloz, C., A. Lai, and T. Itoh, "The challenge of homogenization in metamaterials," *New J. Phys.*, Vol. 7, 167–182, 2005.

13. Caloz, C. and T. Itoh, *Electromagnetic Metamaterials Transmission Line Theory and Microwave Applications*, John Wiley & Sons, Inc. Publication, 2006.

14. Varadan, V. K., K. J. Vinoy, and K. A. Jose, *RF MEMS and Their Applications*, John Wiley & Sons Ltd, 2002.

15. Chicherin, D., M. Sterner, J. Oberhammer, S. Dudorov, J. Åberg, and A. V. Räisänen, "Analog type millimeter wave phase shifters based on MEMS tunable high-impedance surface in rectangular metal waveguide," *IEEE MTT-S Digest,* 61–64, May 23–28, 2010.

16. Pozar, D. M., *Microwave Engineering*, John Wiley & Sons, Inc. Publication, 1998.